Multi-Objective Model Predictive Current Control Method of Permanent Magnet Synchronous Traction Motors with Multiple Current Bounds in Railway Application

Shuai Lin, *Student Member*, *IEEE*, Xiaochun Fang, *Member*, *IEEE*, Xiaofan Wang, Zhongping Yang, *Member*, *IEEE*, and Fei Lin, *Member*, *IEEE*

***Abstract*—For multi-objective model predictive current control method with penalties, the penalty weights are introduced into the cost function to determine the relative importance of control targets. However, the dimensions and value ranges of each control target are different. Thus, the penalty coefficient is difficult to determine. To avoid the difficulty of dimensionless parameter design, this paper proposes a multi-objective control method called model predictive current control with multiple current bounds. In this paper, the switching frequency and the common-mode voltage are selected as the control target. Their control is converted into the limitation of the current ripple so that the control parameters have a clear physical meaning. On the one hand, the proposed method can realize the cooperative control of reference current tracking, switching frequency suppression, and common-mode voltage suppression. On the other hand, the key control parameters have the same dimension and strong correlation with others. Therefore, appropriate parameter design can be realized. Experimental investigations for PMSM prove the effectiveness of the control method.**

***Index Terms*—Permanent magnet synchronous motor (PMSM); model predictive current control (MPCC); switching frequency; common-mode voltage (CMV); current bound limit.**

I. Introduction

With the advantages of high efficiency and high power density, the permanent magnet synchronous motor (PMSM) has been widely applied in rail transit in recent years. The research on PMSM control technology is of great significance to the development of rail transit, and the high-performance control strategy of PMSM has been a research hotspot [1, 2]. Field oriented control (FOC) and direct torque control (DTC) are the two most typical control methods. FOC is usually implemented based on the proportional-integral controller and pulse width modulation (PWM). Its dynamic response is poor at low switching frequency. Besides, parameter tuning and modulation are complex. DTC is usually implemented based on the hysteresis controller, with fast dynamic response but serious current distortion.

In recent years, model predictive control (MPC) has become a research hotspot in the field of power electronic converters and motor drive control [3, 4]. In particular, the research on finite set MPC (FS-MPC) has covered almost all power electronic converters and motor drive systems. The application of MPC in PMSM has the advantages of intuitive concept, algorithmic simplicity, fast dynamic response, ease to deal with multi-variable and multi-constraint cases, and no requirement of modulation [5-7]. Therefore, FS-MPC of PMSM is expected to develop into a new solution for the traction drive control system.

In MPC, the cost function can flexibly describe the control targets. The controlled variables can be torque, current or flux, etc. The corresponding control strategy can be called model predictive torque control (MPTC) [8], model predictive current control (MPCC), etc. Theoretically, a small current ripple can guarantee a small torque ripple, but in turn, a small torque ripple may not guarantee a small current ripple [9]. Therefore, MPTC and MPCC have inherent consistency in motor output torque control, but they are different in the current ripple. This difference is more obvious in low switching frequency applications.

In the railway traction drive system, the maximum switching frequency of the traction inverter is limited. Therefore, MPCC is preferred in railway application. And the switching frequency can be affected and controlled by setting the penalty term of the switching times in the cost function, which can be called MPCC with penalties (MPCC-P) [10]. The cost function will comprehensively consider the two control goals of current reference tracking and switching frequency suppression. Since the dimensions and value ranges of the current error and switching times are different, the weight coefficients have no clear physical meaning and are difficult to design. Based on this conventional multi-objective control method, when it is necessary to increase other control objectives, such as

This work was supported by "the Fundamental Research Funds for the Central Universities" (2019YJS174). (*Corresponding author: Xiaochun Fang*.)

S. Lin, X. Fang, Z. Yang, and F. Lin are with the Beijing Jiaotong University, Beijing, 100044, China (e-mail: ShuaiLin@bjtu.edu.cn; fangxc@bjtu.bjtu.edu.cn; zhpyang@bjtu.edu.cn; flin@bjtu.edu.cn).

X. Wang is with Locomotive & Car Research Institute, China Academy of Railway Sciences Corporation Limited, Beijing, 100081, China (e-mail: wangxiaofan@zemt.cn).

common-mode voltage (CMV) suppression, a new penalty term must be added into the cost function. The design difficulty of the penalty coefficients will be greatly increased, which is not conducive to engineering applications.

The selection of weight coefficients related to multi-objective control has always been a difficult problem that MPC needs to solve. At present, the most common method is to rely on trial and error to test the control effect of different weight coefficient combinations, but this method is very time-consuming [10]. In order to reduce the time cost, [11] proposed to use the branch and bound algorithm to reduce the number of simulations, but the selection of weight coefficients in this process is still empirical. Reference [12] proposed an online adjustment scheme for weight coefficients, which derived the optimal weighting factor based on the torque ripple expression. However, this method is only used to minimize torque ripple, and the switching frequency is not controlled. Besides, complex online calculations increase the burden on the processor. References [13-16] aimed at integrating torque and flux linkage as a control goal in predictive torque control, thus avoiding the problem of weight coefficient selection. But this method is less versatile. Reference [17] construct a cost function by reference voltage vector to achieve model predictive direct speed control without weighting factor. Reference [18] achieved FS-MPC that simultaneously evaluated speed and current control objectives. The weighting factor handling strategy is on the account of the balance of state sensitivity to voltage alteration, which is not suitable for the control of switching frequency. Reference [5, 19] proposed solutions for MPTC to obtain the optimal weighting factors, but MPCC is preferred in railway application. Reference [20] proposed a dynamic function and tuned weighting factors adaptively by fuzzy method to achieve current and switching frequency. However, the switching frequency is too high for railway application. Reference [21] proposed a dynamically weighted optimal switching vector MPC of active rectifier. In recent years, artificial intelligence has been widely applied to design weighting factors, such as artificial neural networks (ANN) [22, 23], particle swarm algorithm [24], and genetic algorithm [25]. Reference [22, 23] employed ANN to select weight coefficients. Numerous simulations or experiments are required to obtain data.

To avoid the problem of dimensionless control parameter design in the conventional MPCC-P, this paper proposes a method called MPCC with bounds (MPCC-B). The control targets are converted into the limitation of the current ripple so that the control parameters have a clear physical meaning. And the quantitative relationship between ripple current boundary, switching frequency, and current distortion is analyzed. The proposed MPCC-B method can not only achieve the control target of the switching frequency, but also does not need to change the original cost function with single control target. The ripple current boundary has a clear physical meaning, and the allowable ripple current of the system can be used as a basis for parameter design. Based on the MPCC-B method, a three-objective cooperative control method with multiple bounds (MPCC-MB) is further proposed. In this paper, the CMV suppression is taken as the third control target to illustrate the three-objective cooperative control method. The proposed MPCC-MB can not only suppress the CMV but also unify the switching frequency control and the CMV suppression under the ripple current boundary. The control parameters corresponding to the switching frequency and CMV have the same dimension and correlation, and the design difficulty is greatly reduced. The multi-objective cooperative control method is similar.

The following sections of this paper are managed as follows. In Section II, the PMSM MPCC control framework and performance evaluation indexes are established. Section III introduces the cooperative control of current distortion and switching frequency. And the three-objective cooperative control is described in Section IV. Section V collates and analyzes the experimental results. Section VI is the conclusion.

II. MPCC OF PMSM TRACTION SYSTEM

A. System Modeling and Predictive Control Framework

The block diagram of the conventional MPCC is shown in Fig. 1. In Fig. 1, i_{sd}^{ref}, i_{sq}^{ref} is the reference currents obtained by looking up the maximum torque per ampere (MTPA) table; i_{sd}, i_{sq} is the actual currents obtained by sampling; v_k^{opt} is the optimal voltage vector selected based on the cost function. The finite set (FS) is composed of the eight basic voltage vectors v_k (k = 0, 1, 2, …, 7) of the three-phase two-level inverter. The FS is shown in TABLE I. S_x (x = a, b, c) is the switch state of the inverter. In order to reduce the switching frequency, only current voltage vector and three adjacent voltage vectors will be applied for the next sampling period.

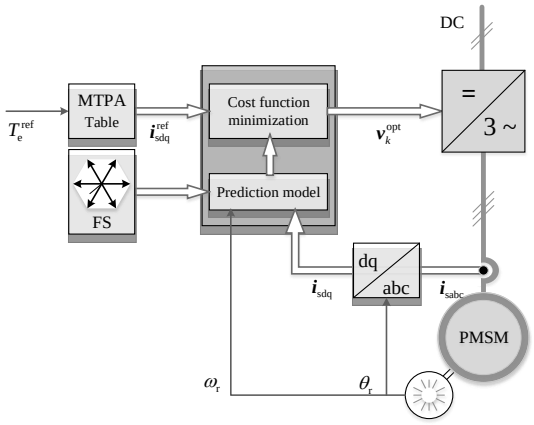

Fig. 1. Block diagram of MPCC.

TABLE I
FS OF MPCC

Current voltage vector $\boldsymbol{v}_k(t_0)$	Switch state (S_a S_b S_c)	Preselected voltage vector set I for the next sampling period
$\boldsymbol{v}_0$	(0 0 0)	$\{\boldsymbol{v}_0\ \boldsymbol{v}_1\ \boldsymbol{v}_3\ \boldsymbol{v}_5\}$
$\boldsymbol{v}_1$	(1 0 0)	$\{\boldsymbol{v}_1\ \boldsymbol{v}_6\ \boldsymbol{v}_2\ \boldsymbol{v}_0\}$
$\boldsymbol{v}_2$	(1 1 0)	$\{\boldsymbol{v}_2\ \boldsymbol{v}_1\ \boldsymbol{v}_3\ \boldsymbol{v}_7\}$
$\boldsymbol{v}_3$	(0 1 0)	$\{\boldsymbol{v}_3\ \boldsymbol{v}_2\ \boldsymbol{v}_4\ \boldsymbol{v}_0\}$
$\boldsymbol{v}_4$	(0 1 1)	$\{\boldsymbol{v}_4\ \boldsymbol{v}_3\ \boldsymbol{v}_5\ \boldsymbol{v}_7\}$
$\boldsymbol{v}_5$	(0 0 1)	$\{\boldsymbol{v}_5\ \boldsymbol{v}_4\ \boldsymbol{v}_6\ \boldsymbol{v}_0\}$
$\boldsymbol{v}_6$	(1 0 1)	$\{\boldsymbol{v}_6\ \boldsymbol{v}_5\ \boldsymbol{v}_1\ \boldsymbol{v}_7\}$
$\boldsymbol{v}_7$	(1 1 1)	$\{\boldsymbol{v}_7\ \boldsymbol{v}_2\ \boldsymbol{v}_4\ \boldsymbol{v}_6\}$

Thus, the framework of convention MPCC mainly includes the following [7]:

(1) calculation of the reference currents;

(2) prediction of the stator currents;

(3) cost function evaluation and minimization.

For MPCC, the establishment of the prediction model and the design of the cost function are the most important. The details of them are described as follows.

The stator voltage equation of PMSM in the rotor reference frame can be written as

$$\begin{aligned} u_{\mathrm{sd}}(t) &= R_{\mathrm{s}} i_{\mathrm{sd}}(t) + L_{\mathrm{sd}} \frac{\mathrm{d}i_{\mathrm{sd}}(t)}{\mathrm{d}t} - \omega_{\mathrm{r}} L_{\mathrm{sq}} i_{\mathrm{sq}}(t) \\ u_{\mathrm{sq}}(t) &= R_{\mathrm{s}} i_{\mathrm{sq}}(t) + L_{\mathrm{sq}} \frac{\mathrm{d}i_{\mathrm{sq}}(t)}{\mathrm{d}t} + \omega_{\mathrm{r}} (L_{\mathrm{sd}} i_{\mathrm{sd}}(t) + \psi_{\mathrm{f}}) \end{aligned} \tag{1}$$

where u_{sd}, u_{sq} are the dq-axis stator voltages; i_{sd}, i_{sq} are the dq-axis stator currents; R_{s} is the stator resistance; L_{d}, L_{q} are the dq-axis inductances; ω_{r} is the electrical rotor speed; ψ_{f} is the permanent magnet flux linkage.

For a sampling interval ($\Delta t = T_{\mathrm{c}}$), (2) can be obtained by first-order Euler's approximation.

$$\frac{di(t)}{dt} \approx \frac{i(t+T_{\mathrm{c}}) - i(t)}{T_{\mathrm{c}}} \tag{2}$$

The prediction model can be obtained from (1) and (2), which is expressed as [26]

$$\begin{aligned} i_{\mathrm{sd}}^{\mathrm{pre}}(t_0+T_{\mathrm{c}},k) &= (1-\frac{R_{\mathrm{s}}T_{\mathrm{c}}}{L_{\mathrm{d}}}) i_{\mathrm{sd}}(t_0) + T_{\mathrm{c}} \frac{L_{\mathrm{q}}}{L_{\mathrm{d}}} \omega_{\mathrm{r}} i_{\mathrm{sq}}(t_0) + \frac{T_{\mathrm{c}}}{L_{\mathrm{d}}} u_{\mathrm{sd}}(t_0,k) \\ i_{\mathrm{sq}}^{\mathrm{pre}}(t_0+T_{\mathrm{c}},k) &= (1-\frac{R_{\mathrm{s}}T_{\mathrm{c}}}{L_{\mathrm{q}}}) i_{\mathrm{sq}}(t_0) - T_{\mathrm{c}} \frac{L_{\mathrm{d}}}{L_{\mathrm{q}}} \omega_{\mathrm{r}} i_{\mathrm{sd}}(t_0) + \frac{T_{\mathrm{c}}}{L_{\mathrm{q}}} u_{\mathrm{sq}}(t_0,k) \\ &\quad - \omega_{\mathrm{r}} \psi_f T_{\mathrm{c}} \end{aligned} \tag{3}$$

where $i_{\mathrm{sd}}^{\mathrm{pre}}$, $i_{\mathrm{sq}}^{\mathrm{pre}}$ are the predicted dq-axis currents; k is the voltage vector index of FS; t_0 is the current time; T_{c} is the control period (sampling period).

According to the prediction model (3), the predicted currents can be calculated when different voltage vectors are applied. To compensate for the delay problem, (3) can be rewritten as

$$\begin{aligned} i_{\mathrm{sd}}^{\mathrm{pre}}(t_0+2T_{\mathrm{c}},k) &= (1-\frac{R_{\mathrm{s}}T_{\mathrm{c}}}{L_{\mathrm{d}}}) i_{\mathrm{sd}}(t_0+T_{\mathrm{c}}) + T_{\mathrm{c}} \frac{L_{\mathrm{q}}}{L_{\mathrm{d}}} \omega_{\mathrm{r}} i_{\mathrm{sq}}(t_0+T_{\mathrm{c}}) \\ &\quad + \frac{T_{\mathrm{c}}}{L_{\mathrm{d}}} u_{\mathrm{sd}}(t_0+T_{\mathrm{c}},k) \\ i_{\mathrm{sq}}^{\mathrm{pre}}(t_0+2T_{\mathrm{c}},k) &= (1-\frac{R_{\mathrm{s}}T_{\mathrm{c}}}{L_{\mathrm{q}}}) i_{\mathrm{sq}}(t_0+T_{\mathrm{c}}) - T_{\mathrm{c}} \frac{L_{\mathrm{d}}}{L_{\mathrm{q}}} \omega_{\mathrm{r}} i_{\mathrm{sd}}(t_0+T_{\mathrm{c}}) \\ &\quad + \frac{T_{\mathrm{c}}}{L_{\mathrm{q}}} u_{\mathrm{sq}}(t_0+T_{\mathrm{c}},k) - \omega_{\mathrm{r}} \psi_f T_{\mathrm{c}} \end{aligned} \tag{4}$$

The primary control goal is the reference current tracking. Therefore, the cost function is expressed as

$$J(t,k) = e_{i,\mathrm{sd}}^{\mathrm{pre}\,2}(t,k) + e_{i,\mathrm{sq}}^{\mathrm{pre}\,2}(t,k) \tag{5}$$

where $e_{i,\mathrm{sd}}^{\mathrm{pre}}$ are $e_{i,\mathrm{sq}}^{\mathrm{pre}}$ are the errors between reference currents and predicted currents. They are defined as

$$\begin{cases} e_{i,\mathrm{sd}}^{\mathrm{pre}}(t,k) = i_{\mathrm{sd}}^{\mathrm{ref}}(t,k) - i_{\mathrm{sd}}^{\mathrm{pre}}(t,k) \\ e_{i,\mathrm{sq}}^{\mathrm{pre}}(t,k) = i_{\mathrm{sq}}^{\mathrm{ref}}(t,k) - i_{\mathrm{sq}}^{\mathrm{pre}}(t,k) \end{cases} \tag{6}$$

The voltage vector which makes cost function J minimum is selected as the optimal voltage vector $v_{\mathrm{k}}^{\mathrm{opt}}$. In (7), arg minimize means the solution of $v_k(t_0+T_{\mathrm{c}})$ that makes $J(t_0+2T_{\mathrm{c}},k)$ minimum.

$$\boldsymbol{v}_k^{\mathrm{opt}}(t_0+T_{\mathrm{c}}) = \arg \underset{\boldsymbol{v}_k(t_0+T_{\mathrm{c}})}{\text{minimize}}\ J(t_0+2T_{\mathrm{c}},k) \tag{7}$$

B. Performance Evaluation Indexes

For railway application, power loss and switching frequency are important factors that affect the traction system performance. In order to reduce the power loss, the harmonic distortion of the stator current must be minimized. Total demand distortion (TDD) of stator current can be expressed as

$$I_{\mathrm{TDD}} = \frac{1}{\sqrt{2} I_{\mathrm{s,nom}}} \sqrt{\sum_{n\neq 1} (i_{\mathrm{s},n})^2} \tag{8}$$

where $I_{\mathrm{s,nom}}$ represents the effective value of rated current; $i_{\mathrm{s},n}$ represents the amplitude of the n_{th} harmonic current.

Within N sampling cycles, the total switching times of the inverter are summed. Then they are divided by the time and the number of power modules to estimate the average switching frequency. Therefore, the average switching frequency can be expressed as

$$f_{\mathrm{sw}} = \lim_{N\to\infty} \frac{1}{6NT_{\mathrm{c}}} \sum_{x=\mathrm{a,b,c}} \sum_{l=1}^{N} \left| S_x(t_0+lT_{\mathrm{c}}) - S_x(t_0+lT_{\mathrm{c}}-T_{\mathrm{c}}) \right| \tag{9}$$

Since the switching frequency of MPC is not fixed, it is difficult to compare the current TDD at the same switching frequency. Consequently, the product C_{sw} of I_{TDD} and f_{sw} is used as a comprehensive evaluation index for current distortion and switching frequency

$$C_{\mathrm{sw}} = I_{\mathrm{TDD}} \cdot f_{\mathrm{sw}} \tag{10}$$

The smaller the C_{sw} is, the better the current waveform is obtained with less switching times, and the better the control performance is.

In order to introduce the three-objective cooperative control, the CMV is taken as an example of the third control target. The effective value of common-mode voltage U_{com} is defined as

$$U_{\mathrm{com}} = \sqrt{\frac{1}{T_1} \int_0^{T_1} u_{\mathrm{com}}^2(t)\mathrm{d}t} \tag{11}$$

where u_{com} is the instantaneous value of the common-mode voltage, T_1 is the fundamental period.

III. Cooperative Control of Current Distortion and Switching Frequency

For MPCC-P, a penalty term of switching times is added into the cost function to achieve the control of switching frequency. The cost function is expressed as

$$J(t,k) = e_{i,\mathrm{sd}}^{\mathrm{pre}\,2}(t,k) + e_{i,\mathrm{sq}}^{\mathrm{pre}\,2}(t,k) + \lambda_{\mathrm{sw}} n_{\mathrm{sw}}(t,k) \tag{12}$$

where n_{sw} is the switching times in each control cycle, and λ_{sw} is the switching frequency penalty coefficient. The voltage vector which makes the cost function minimum is selected to realize the cooperative control of current distortion and switching frequency.

The switching frequency can be reduced by increasing the value of λ_{sw}, but the key problem is that the penalty coefficient λ_{sw} is difficult to determine. The dimensions and value ranges of current error and switching times are different. The switching frequency penalty coefficient λ_{sw} is a dimensionless control parameter, which has no clear physical meaning and is difficult to design.

This paper proposes a method based on ripple current bounds limit to realize the decoupling of switching frequency and control frequency, which is called MPCC-B. The control

framework is shown in Fig. 2. The cost function only realizes the reference current tracking and its expression is shown as (5). The control of switching frequency is realized by the boundary limit module in Fig. 2. In other words, the control of switching frequency is converted into the limitation of the current ripple. After the optimal voltage vector is selected by minimizing the cost function, it is determined whether to update the switching state of the inverter according to whether the boundary is reached.

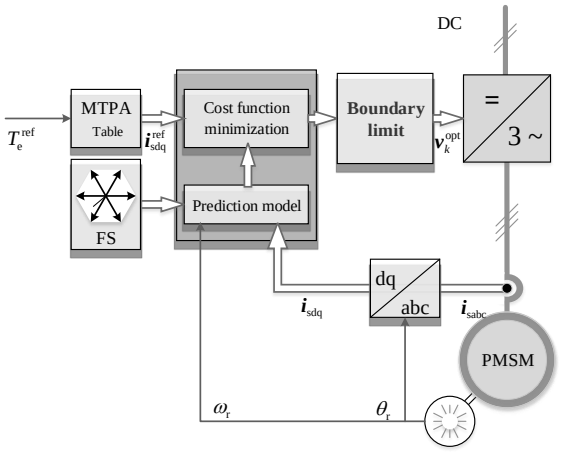

Fig. 2. Block diagram of model predictive current control with bounds.

In the preselected voltage vector set (TABLE I), there are total four voltage vectors, the first of which is the current voltage vector $v_k(t_0)$, and the other three are voltage vectors adjacent to $v_k(t_0)$. Therefore, in each sampling period, the number of switching times of the inverter is 0 or 1. The selection of optimal voltage vector is based on the relationship between predicted current error $e_{i,s}^{pre}(t_0+2T_c, v_k(t_0))$ and the set current ripple boundary radius $e_{i,sw}$, and (13) shows the selection rule.

$$\boldsymbol{v}_k^{opt}(t_0+T_c)=\begin{cases}\boldsymbol{v}_k^{opt}(t_0), & e_{i,s}^{pre}\left(t_0+2T_c,k(t_0)\right)\le e_{i,sw}\\ \underset{\boldsymbol{v}_k(t_0+T_c)}{\arg\ \text{minimize}}\ J(t_0+2T_c,k), & e_{i,s}^{pre}\left(t_0+2T_c,k(t_0)\right)> e_{i,sw}\end{cases} \quad (13)$$

Under this voltage vector selection mechanism, the sampling frequency can be increased as much as possible with sufficient computation time. And the control accuracy can be improved. The switching state of the inverter can remain unchanged for a period of time Δt until the predicted current trajectory touches the boundary. By setting the size of the ripple current boundary radius $e_{i,sw}$, the switching frequency can be adjusted. What's more, the control parameter $e_{i,sw}$ also has a clear physical meaning. It means the current fluctuation that the system can tolerate. This feature makes the parameter design of the MPCC-B method more convenient than the MPCC-P method.

IV. Three-Objective Cooperative Control Considering Common-Mode Voltage Method

The three-objective cooperative control method follows a similar principle. The CMV of inverters is one of the causes of bearing damage and electromagnetic interference issues. Therefore, the CMV suppression is taken as an example of the third control target to illustrate the three-objective cooperative control method. For MPCC-P, the penalty coefficient λ_{com} is introduced, and the cost function (12) is modified to

$$J(t,k)=e_{i,sd}^{pre\,2}(t,k)+e_{i,sq}^{pre\,2}(t,k)+\lambda_{sw}n(t,k)+\lambda_{com}\left|u_{com}(t,k)\right| \quad (14)$$

When λ_{sw} is constant, the larger λ_{com} is, the stronger the CMV suppression effect is. Since the dimensions and value ranges of current, switching times, and CMV are completely different, the difficulty of penalty coefficient design is greatly increased.

A. CMV Suppression Based on Multiple Bound Limit

Based on MPCC-B, the suppression of CMV is further added, and MPCC-MB is proposed. In MPCC-MB, there are two bound limit values, which are the switching frequency boundary limit $e_{i,sw,}$ and the CMV boundary limit $e_{i,com}$. The selection process of the optimal voltage vector is shown in Fig. 3. It includes the following:

(1) estimating the current error at the next sampling time;

(2) predicting the current error based on preselected vector set I (TABLE I);

(3) correcting the preselected vector set II (TABLE II);

(4) minimizing the cost function based on the preselected vector set (TABLE II).

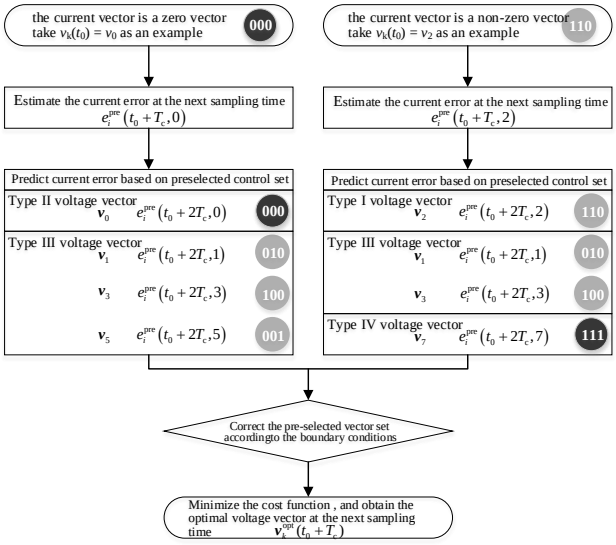

Fig. 3. Optimize voltage vector selection of MPCC-MB.

According to the different effects of each voltage vector on the switching frequency and CMV, the preselected voltage vector set can be divided into the following four categories:

Type I voltage vector: The number of switching times is 0, and the CMV amplitude is $U_{dc}/3$. U_{dc} is half of the DC-link voltage.

Type II voltage vector: The number of switching times is 0, and the CMV amplitude is U_{dc}.

Type III voltage vector: The number of switching times is 1, and the CMV amplitude is $U_{dc}/3$.

Type IV voltage vector: The number of switching times is 1, and the CMV amplitude is U_{dc}.

When selecting the optimal voltage vector, the above four categories are arranged from high to low in the order of priority as I> II> III> IV to achieve the purpose of reducing the switching frequency and CMV. In the control logic, the priority of switching frequency control is higher than CMV control.

According to the type of the current voltage vector $v_k(t_0)$, it can be divided into the following two cases:

(1) If the current vector is a zero vector (take $v_k(t_0) = v_0$ as an example), the current zero vector v_0 is a type II voltage vector, and the remaining three non-zero vectors (v_1, v_3, and v_5) are type III vectors.

(2) If the current vector is a non-zero vector (take $v_k(t_0) = v_2$ as an example), the current vector v_2 is a type I voltage vector, and the two adjacent non-zero voltage vectors (v_1 and v_3) are type III vectors. The zero voltage vector (v_7) is a type IV vector.

After obtaining $e_{i,s}^{\text{pre}}(t_0+2T_c,k)$, the preselected vector set is modified by comparing their amplitudes with bound limit radius $e_{i,\text{sw}}$, $e_{i,\text{com}}$. The modification rules are shown in TABLE II. If the predicted current error of the current voltage vector is smaller than the switching frequency boundary limit, the preselected vector set II only includes the current voltage vector. If the predicted current error of the current voltage vector is larger than the switching frequency boundary limit, the control of CMV will be considered and the preselected vector set II will include more voltage vectors.

TABLE II
MODIFICATIONS OF PRESELECTED SETS OF BASIC VOLTAGE VECTORS

Current voltage vector	Switching frequency boundary limit	CMV boundary limit	Preselected vector set II
$\boldsymbol{v}_0$	$e_{i,s}^{\text{pre}}(t_0+2T_c,0) < e_{i,\text{sw}}$	No	$\{\boldsymbol{v}_0\}$
	$e_{i,s}^{\text{pre}}(t_0+2T_c,0) \geq e_{i,\text{sw}}$	No	$\{\boldsymbol{v}_0\ \boldsymbol{v}_1\ \boldsymbol{v}_3\ \boldsymbol{v}_5\}$
$\boldsymbol{v}_2$	$e_{i,s}^{\text{pre}}(t_0+2T_c,2) < e_{i,\text{sw}}$	No	$\{\boldsymbol{v}_2\}$
	$e_{i,s}^{\text{pre}}(t_0+2T_c,2) \geq e_{i,\text{sw}}$	$e_{i,s}^{\text{pre}}(t_0+2T_c,1\text{or}3) < e_{i,\text{com}}$	$\{\boldsymbol{v}_2\ \boldsymbol{v}_1\ \boldsymbol{v}_3\}$
	$e_{i,s}^{\text{pre}}(t_0+2T_c,2) \geq e_{i,\text{sw}}$	$e_{i,s}^{\text{pre}}(t_0+2T_c,1\text{or}3) \geq e_{i,\text{com}}$	$\{\boldsymbol{v}_2\ \boldsymbol{v}_1\ \boldsymbol{v}_3\ \boldsymbol{v}_7\}$

According to Fig. 3 and TABLE II, the optimal voltage vector is obtained by minimizing the cost function based on the modified preselected vector set II. There are two cases for the composition of the preselected vector set I. If the current vector is a zero vector, the preselected voltage vector includes one type II vector and three types III vectors; if the current vector is a non-zero vector, the preselected voltage vector includes one type I vector, two III vectors and one type IV vector.

B. The Law of The Size of The Multiple Bounds

In MPCC-P, the relationship between the control targets in the cost function is completely parallel. The setting of the switching frequency penalty coefficient λ_{sw} and the CMV penalty coefficient λ_{com} will affect each other, but there is no clear corresponding relationship between their value ranges.

In MPCC-MB, $e_{i,\text{sw}}$ can be smaller than $e_{i,\text{com}}$, or larger, or equal. However, according to preselected vector modification rules in TABLE II, the priority of switching frequency is higher than CMV. After the values of $e_{i,\text{sw}}$ is determined, the value range of $e_{i,\text{com}}$ can also be roughly determined.

In a sampling interval, there will be a maximum value for the variation of current error, which is set to $|\Delta e_{i,\max}|$. First, consider the case when $e_{i,\text{com}}$ is too small, that is

$$e_{i,\text{com}} < e_{i,\text{sw}} - \left|\Delta e_{i,\max}\right| \tag{15}$$

When the predicted current error touches the boundary $e_{i,\text{sw}}$, a state switch needs to be activated. However, the predicted current errors corresponding to all vectors are all outside the CMV boundary, that is

$$e_{i,s}^{\text{pre}}\left(t_0+2T_c,k\right) > e_{i,\text{com}} \tag{16}$$

Therefore, the CMV suppression boundary is invalid at this time, and its control effect is equivalent to not performing CMV suppression at all.

Similarly, consider the case when $e_{i,\text{com}}$ is too large, that is

$$e_{i,\text{com}} > e_{i,\text{sw}} + \left|\Delta e_{i,\max}\right| \tag{17}$$

And the predicted current errors corresponding to all vectors are all within the CMV boundary, that is

$$e_{i,s}^{\text{pre}}\left(t_0+2T_c,k\right) < e_{i,\text{com}} \tag{18}$$

Therefore, the CMV suppression boundary is invalid, and its control effect is equivalent to completely abandoning the zero vector, and the CMV will always remain $U_{\text{dc}}/3$.

Consequently, under a certain switching frequency boundary $e_{i,\text{sw}}$, the value range of the CMV boundary $e_{i,\text{com}}$ is

$$e_{i,\text{sw}} - \left|\Delta e_{i,\max}\right| < e_{i,\text{com}} < e_{i,\text{sw}} + \left|\Delta e_{i,\max}\right| \tag{19}$$

V. EXPERIMENT

A. Experimental Platform

The experimental platform is shown in Fig. 4. It consists of an induction motor and a PMSM. The two motors are connected through a coupling. The topology of the experimental platform is shown in Fig. 5. PMSM driven by inverter 1 is used as the traction motor. The dSPACE real-time simulation system is used as the controller of inverter 1. Inverter 2 drives the induction motor as a test system. Inverters 1 and 2 are derived from AC-DC-AC converters. Each converter includes a diode three-phase rectifier bridge, an IGBT three-phase two-level inverter, and DC-link capacitors. Since the diode rectifier bridge cannot realize the electric braking energy feedback, the DC-link of the two converters are connected, and the three-phase power supply of 380V and 50Hz is converted by the transformer as the AC input of one of the AC-DC-AC converters.

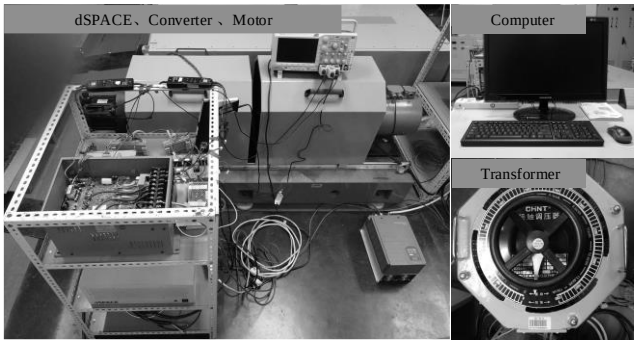

Fig. 4. 4.4 kW experimental platform.

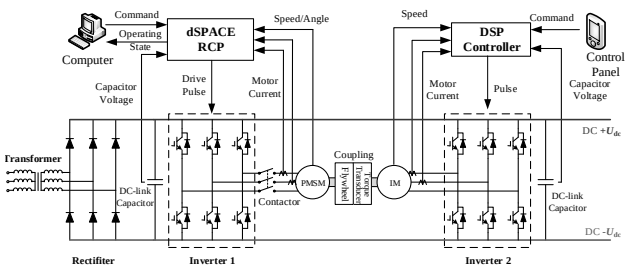

Fig. 5. The topology of 4.4 kW experimental platform.

The main parameters of PMSM are shown in TABLE III. Limited by the laboratory space, in order to ensure safety, the inverter DC-link voltage is adjusted to $2U_{\text{dc}} = 200$ V. The rated frequency of PMSM is about 80 Hz and the rated speed is 960

rpm calculated according to no-load back electromotive force (EMF). The sampling frequency is 40kHz.

TABLE III
PARAMETERS OF PMSM TRACTION SYSTEM

Parameter	Value	Parameter	Value
Rated power /kW	4.4	Magnetic flux linkage /Wb	0.181
Rated speed/rpm	1500	Stator resistance /Ω	0.3
Rated frequency/Hz	125	d-axis inductance /H	0.004
Rated torque/N·m	28.4	q-axis inductance /H	0.0045
Rated voltage/V	380	Pole pair	5
Rated current/A	16.5	DC side voltage /V	200

B. Cooperative Control of Current Distortion and Switching Frequency

In MPCC-B with a sampling frequency of 40kHz, the experiments are carried out under rated frequency (80Hz) and 1/4 rated frequency (20Hz), full load (16A) and 1/2 load (8A), respectively. In each operation condition, the switching frequency boundary $e_{i,\mathrm{sw}}$ increases from 0A to 5A. I_{TDD}, f_{sw}, C_{sw}, and U_{com} are recorded. Fig. 6 shows the experimental results of the evaluation indicators varying with the switching frequency boundary $e_{i,\mathrm{sw}}$. The I_{TDD} increases with the increase of the switching frequency boundary $e_{i,\mathrm{sw}}$, and the switching frequency f_{sw} decreases with the increase of the switching frequency boundary $e_{i,\mathrm{sw}}$.

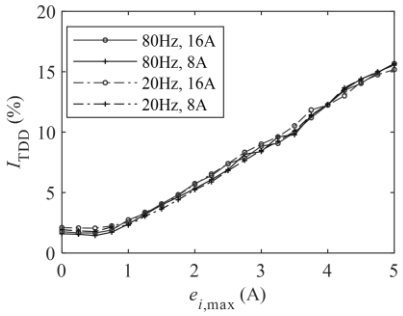

(a) Current TDD I_{TDD}.

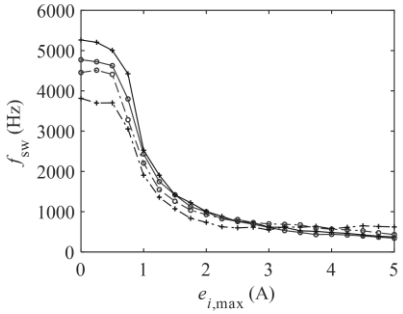

(b) Switching frequency f_{sw}.

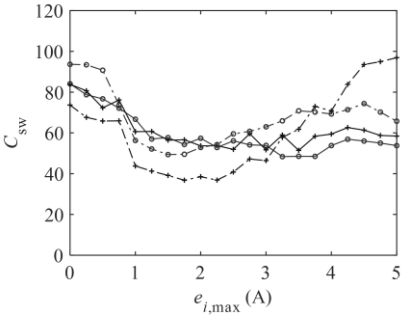

(c) Product C_{sw} of current TDD and switching frequency.

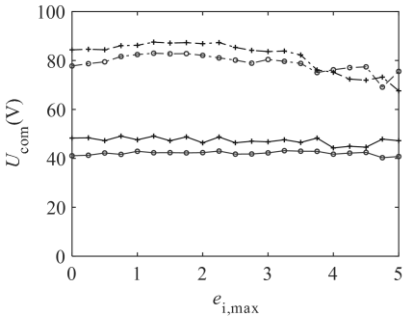

(d) CMV U_{com}.

Fig. 6. The influence of $e_{i,\mathrm{sw}}$ on performance indexes.

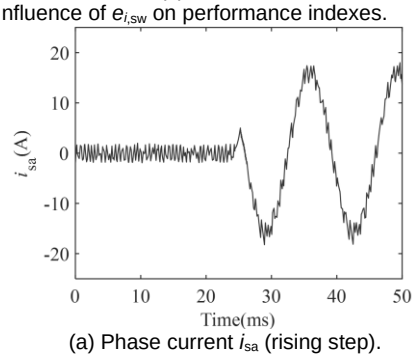

(a) Phase current i_{sa} (rising step).

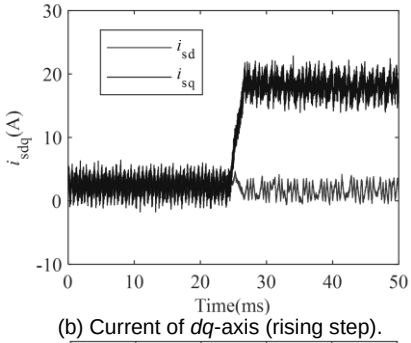

(b) Current of *dq*-axis (rising step).

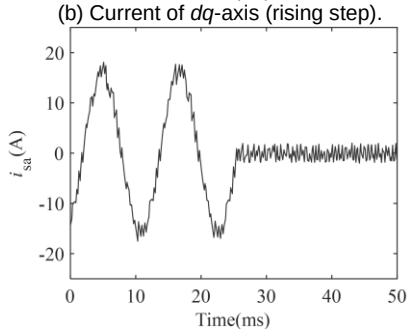

(c) Phase current i_{sa} (falling step).

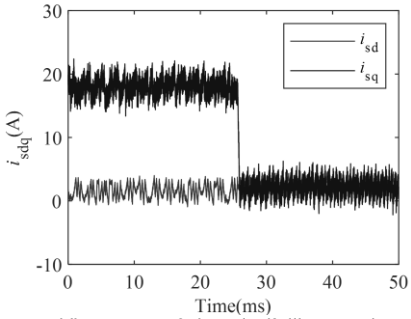

(d) Current of *dq*-axis (falling step).

Fig. 7. Experimental results of MPCC-B with $e_{i,\mathrm{sw}}$ = 2.25 A.

When 0A≤$e_{i,\mathrm{sw}}$<0.75A, with the $e_{i,\mathrm{sw}}$ gradually increase, I_{TDD} and f_{sw} will not change significantly. Although the current

quality is good, the switching frequency is too high to be applicable for railway application. When $e_{i,sw}$≥4.5A, although the switching frequency is very low, the current quality is too poor to be applicable. Although the CMV U_{com} at low speed (20Hz operation condition) in the third stage (2.75A≤ $e_{i,sw}$<4.5A) drops slightly, C_{sw} in the third stage is larger than that in the second stage (0.75A≤ $e_{i,sw}$<2.75A). Consequently, the second stage is preferred and $e_{i,sw}$=2.25A is selected considering that the maximum frequency is no more than 1kHz in traction inverter.

Fig. 7 shows the A-phase current and *dq*-axis currents when $e_{i,sw}$=2.25A. The experimental conditions are: the fundamental frequency is 80Hz, the speed is 960rpm, and the rising step (0→16A) and the falling step (16→0A) are given at 25ms. The adjustment times of the rising and falling steps are 3ms and 1ms.

C. Three-Objective Cooperative Control Considering CMV

In MPCC-MB with a sampling frequency of 40kHz, the experiments are carried out under rated frequency (80Hz) and 1/4 rated frequency (20Hz), full load (16A) and 1/2 load (8A), respectively. Besides, according to (19), the CMV boundary $e_{i,com}$ is around the switching frequency boundary $e_{i,sw}$. $e_{i,sw}$ is set to 2.25A. Therefore, the CMV boundary $e_{i,com}$ increases from 1A to 3A in each operation condition. And I_{TDD}, f_{sw} and U_{com} are recorded.

The experimental results in Fig. 8 show the performance indicators varying with CMV boundary $e_{i,com}$ when $e_{i,sw}$=2.25A. At the rated frequency, when $e_{i,com}$<1.75A, the effective value of CMV at full load and 1/2 load remains unchanged at 42.69V and 50.02V respectively. When 1.75A≤ $e_{i,com}$<2.75A, as the CMV boundary increases, the CMV gradually decreases to the lowest point 31.80V and 32.38V. The lowest point of CMV U_{com} under the four operation conditions is U_{dc}/3. Since the DC voltage varies during the experiment, the lowest point of CMV U_{com} in each condition is slightly different.

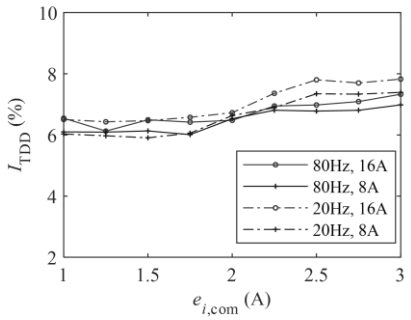

(a) Current TDD I_{TDD}

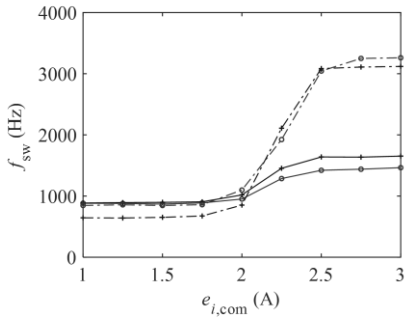

(b) Switching frequency f_{sw}

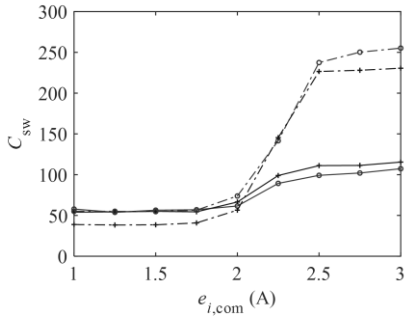

(c) Product of current TDD and switching frequency C_{sw}

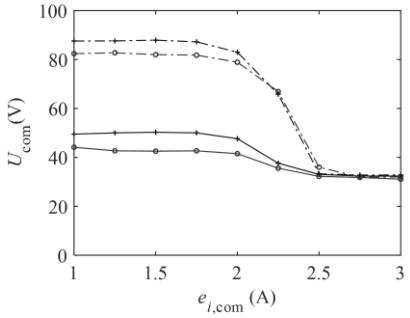

(d) CMV U_{com}

Fig. 8. Experiments of the influence of $e_{i,com}$ on performance indexes.

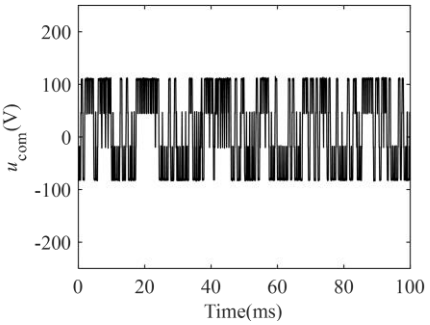

(a) 20Hz, $e_{i,com}$=1.5A

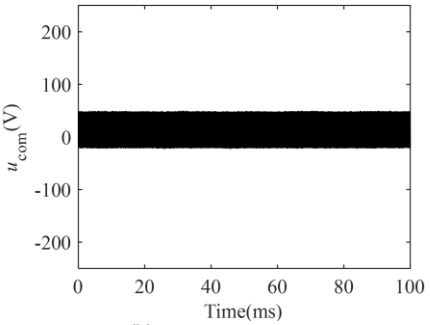

(b) 20Hz, $e_{i,com}$=3.0A

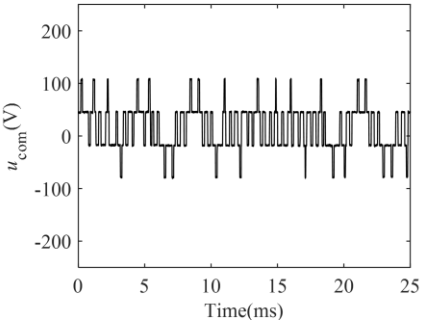

(c) 80Hz, $e_{i,com}$=1.5A

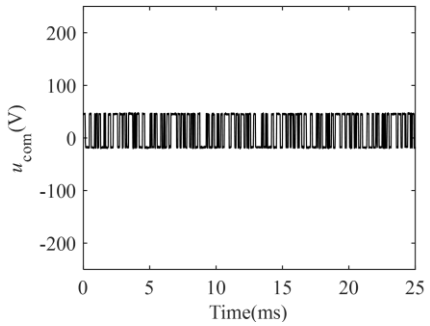

(d) 80Hz, $e_{i,com}$=3.0A

Fig. 9. CMV of MPCC-MB method with $e_{i,sw}$ = 2.25 A.

While the CMV suppression effect is gradually increasing, the current control performance is gradually getting worse. For example, under the rated frequency, I_{TDD} increases from 6.42% to 7.09%, f_{sw} increases from 888Hz to 1439Hz, and C_{sw} increases from 57 to 102 at full load. According to the requirements of different performance evaluation indexes in actual application, $e_{i,com}$ can be set.

Fig. 9 shows CMV when $e_{i,sw}$=2.25A. In the experiment, $|\Delta e_{i,max}|$=0.75A. Fig. 9 (a) and (b) are at 1/4 rated frequency; Fig. 9 (c) and (d) are at rated frequency; in Fig. 9 (a) and (c), $e_{i,com}$=1.5A; in Fig. 9 (b) and (d), $e_{i,com}$=3.0A. For (a) and (c), $e_{i,com}-e_{i,sw}$=-0.75A=-$|\Delta e_{i,max}|$. There is no CMV suppression effect. It can be seen that CMV U_{com} has four states of $\pm U_{dc}$ and $\pm U_{dc}/3$ ($U_{dc} \approx$ 100V in the experiment). For (b) and (d), $e_{i,com}-e_{i,sw}$=0.75A=$|\Delta e_{i,max}|$. The CMV suppression effect is the strongest, and the CMV U_{com} at both speeds is only $\pm U_{dc}/3$. Since $e_{i,sw,}$ and $e_{i,com}$ represent the errors between the predicted current and the reference current, it is easy to adjust the suppression strength of the CMV according to the difference between $e_{i,sw,}$ and $e_{i,com}$.

VI. Conclusion

MPCC-B is established to realize cooperative control of reference current tracking and switching frequency. The problem of switching frequency control is transformed into the limitation of the current ripple, so that the control parameters have a clear physical meaning. Considering multi-objective control, MPCC-MB is further proposed based on MPCC-B. On the one hand, it shows the scalability of MPCC-B. On the other hand, it shows the advantages of MPCC-B over MPCC-P in the design of multi-objective control parameters. In MPCC-MB, the two key control parameters corresponding to the switching frequency and the CMV have the same dimension and have a strong correlation with each other. Thus, blindness in the parameter design process can be avoided. The design theory of MPCC-MB can be widely applied to motor multi-objective control in a variety of application. And the control targets are also not limited to the switching frequency and CMV.

References

[1] K. Kondou and K. Matsuoka, "Permanent magnet synchronous motor control system for railway vehicle traction and its advantages," *Proc. Int. Power Conversion Conference - Nagaoka 1997*, vol.1, pp. 63-68.

[2] I. Spina, A. D. Pizzo, L. Beneduce, B. Cascone, and L. Fratelli, "Comparative analysis of performance and energy losses in light railways vehicles equipped with IM or PMSM drive," *Proc. Int. International Symposium on Power Electronics, Electrical Drives, Automation and Motion*, 2014, pp. 566-572.

[3] S. VAZQUEZ, J. RODRIGUEZ, M. RIVERA, et al. "Model Predictive Control for Power Converters and Drives: Advances and Trends," in *IEEE Transactions on Industrial Electronics*, 2017, 64(2): 935-947.

[4] P. CORTES, M P. KAZMIERKOWSKI, R M. KENNEL, et al. "Predictive Control in Power Electronics and Drives," in *IEEE Transactions on Industrial Electronics*, 2008, 55(12): 4312-4324.

[5] T. Geyer, "Algebraic Tuning Guidelines for Model Predictive Torque and Flux Control," in *IEEE Transactions on Industry Applications*, vol. 54, no. 5, pp. 4464-4475, Sept.-Oct. 2018.

[6] M. F. Elmorshedy, W. Xu, F. F. M. El-Sousy, M. R. Islam and A. A. Ahmed, "Recent Achievements in Model Predictive Control Techniques for Industrial Motor: A Comprehensive State-of-the-Art," in *IEEE Access*, vol. 9, pp. 58170-58191, 2021.

[7] S. G. Petkar, K. Eshwar and V. K. Thippiripati, "A Modified Model Predictive Current Control of Permanent Magnet Synchronous Motor Drive," in *IEEE Transactions on Industrial Electronics*, vol. 68, pp. 1025-1034, Feb. 2021.

[8] M. PREINDL, S. BOLOGNANI. "Model Predictive Direct Torque Control With Finite Control Set for PMSM Drive Systems, Part 1: Maximum Torque Per Ampere Operation," in *IEEE Transactions on Industrial Informatics*, 2013, 9(4): 1912-1921.

[9] J. HOLTZ. "Advanced PWM and Predictive Control—An Overview," in *IEEE Transactions on Industrial Electronics*, 2016, 63(6): 3837-3844.

[10] R. VARGAS, P. CORTES, U. AMMANN, et al. "Predictive Control of a Three-Phase Neutral-Point-Clamped Inverter," in *IEEE Transactions on Industrial Electronics*, 2007, 54(5): 2697-2705.

[11] P. CORTES, S. KOURO, B L. ROCCA, et al. "Guidelines for weighting factors design in Model Predictive Control of power converters and drives," *2009 IEEE International Conference on Industrial Technology*, 10-13 Feb. 2009, Gippsland, VIC, Australia. IEEE, 2009: 1-7.

[12] S A. DAVARI, D A. KHABURI, R. KENNEL. "An Improved FCS–MPC Algorithm for an Induction Motor With an Imposed Optimized Weighting Factor," in *IEEE Transactions on Power Electronics*, 2012, 27(3): 1540-1551.

[13] E. FUENTES, C A. SILVA, R M. KENNEL. "MPC Implementation of a Quasi-Time-Optimal Speed Control for a PMSM Drive, With Inner Modulated-FS-MPC Torque Control," in *IEEE Transactions on Industrial Electronics*, 2016, 63(6): 3897-3905.

[14] F. WANG, H. XIE, Q. CHEN, et al. "Parallel Predictive Torque Control for Induction Machines Without Weighting Factors," in *IEEE Transactions on Power Electronics*, 2020, 35(2): 1779-1788.

[15] C. Ma et al., "A Novel Torque Boundary-Based Model Predictive Torque Control for PMSM Without Weighting Factor," in *IEEE Journal of Emerging and Selected Topics in Power Electronics*, vol. 9, no. 4, pp. 4395-4406, Aug. 2021.

[16] Z. Zhang, Q. Sun, Q. Di and Y. Wu, "A Predictive Torque Control Method for Dual Three-Phase Permanent Magnet Synchronous Motor Without Weighting Factor," in *IEEE Access*, vol. 9, pp. 112585-112595, 2021.

[17] X. Zhang and Y. He, "Direct Voltage-Selection Based Model Predictive Direct Speed Control for PMSM Drives Without Weighting Factor," in *IEEE Transactions on Power Electronics*, vol. 34, no. 8, pp. 7838-7851, Aug. 2019.

[18] Y. Han, C. Gong, L. Yan, H. Wen, Y. Wang and K. Shen, "Multiobjective Finite Control Set Model Predictive Control Using Novel Delay Compensation Technique for PMSM," in *IEEE Transactions on Power Electronics*, vol. 35, no. 10, pp. 11193-11204, Oct. 2020.

[19] M. H. Arshad, M. A. Abido, A. Salem and A. H. Elsayed, "Weighting Factors Optimization of Model Predictive Torque Control of Induction Motor Using NSGA-II With TOPSIS Decision Making," in *IEEE Access*, vol. 7, pp. 177595-177606, 2019.

[20] Z. Chen, W. Tu, L. Yan and G. Luo, "Dynamic Cost Function Design of Finite-Control-Set Model Predictive Current Control for PMSM Drives," *2019 IEEE International Symposium on Predictive Control of Electrical Drives and Power Electronics (PRECEDE)*, 2019, pp. 1-6.

[21] L. M. A. Caseiro, A. M. S. Mendes and S. M. A. Cruz, "Dynamically Weighted Optimal Switching Vector Model Predictive Control of Power Converters," in *IEEE Transactions on Industrial Electronics*, vol. 66, no. 2, pp. 1235-1245, Feb. 2019.

[22] T. DRAGICEVIC, M. NOVAK. "Weighting Factor Design in Model Predictive Control of Power Electronic Converters: An Artificial Neural

Network Approach," in *IEEE Transactions on Industrial Electronics*, 2018: 1-1.

[23] M. Novak, H. Xie, T. Dragicevic, F. Wang, J. Rodriguez and F. Blaabjerg, "Optimal Cost Function Parameter Design in Predictive Torque Control (PTC) Using Artificial Neural Networks (ANN)," in *IEEE Transactions on Industrial Electronics*, vol. 68, no. 8, pp. 7309-7319, Aug. 2021.

[24] H. Fretes et al., "Pareto Optimal Weighting Factor Design of Predictive Current Controller of a Six-Phase Induction Machine based on Particle Swarm Optimization Algorithm," in *IEEE Journal of Emerging and Selected Topics in Power Electronics*.

[25] P. R. U. Guazzelli, W. C. de Andrade Pereira, C. M. R. de Oliveira, A. G. de Castro and M. L. de Aguiar, "Weighting Factors Optimization of Predictive Torque Control of Induction Motor by Multiobjective Genetic Algorithm," in *IEEE Transactions on Power Electronics*, vol. 34, no. 7, pp. 6628-6638, July 2019.

[26] X. Wang, X. Fang, F. Lin and Z. Yang, "Predictive current control of permanent-magnet synchronous motors for rail transit including quasi six-step operation," *2017 IEEE Transportation Electrification Conference and Expo, Asia-Pacific (ITEC Asia-Pacific)*, 2017, pp. 1-6.

Shuai Lin (S'19) received the B.S. degree in electrical engineering from Beijing Jiaotong University, Beijing, China, in 2017, where he is currently pursuing the Ph.D. degree with the School of Electrical Engineering.

His current research interests include motor drives and reliability of traction drive systems.

Xiaochun Fang (S'14–M'17) received the B.S. and Ph.D. degrees in engineering from Beijing Jiaotong University, Beijing, China, in 2010 and 2016, respectively.

He is currently a Associate Professor with the School of Electrical Engineering, Beijing Jiaotong University. His current research interests include traction converters and motor drives, energy management for railway systems, IGBT fault mechanisms, and failure prediction.

Xiaofan Wang received the B.S. and Ph.D degree from Beijing Jiaotong University, Beijing China, in 2014 and 2020, respectively, both in electrical engineering.

He is currently a Research Associate with the Locomotive & Car Research Institute, China Academy of Railway Sciences Corporation Limited, Beijing, China. His research interests include traction converter and motor drives, digital control of power-electronic-based devices.

Zhongping Yang (M'14) received the B.Eng. degree from Tokyo University of Mercantile Marine, Tokyo, Japan in 1997, and reveived the M.Eng. degree and Ph.D. degree from the University of Tokyo, Tokyo, Japan in 1999 and 2002 respectively, all in electrical engineering.

He is currently a Professor in the School of Electrical Engineering, Beijing Jiaotong University, Beijing, China. His research interests include high-speed rail integration technology, traction & regenerative braking technology, and wireless power transfer of urban rail vehicles.

Fei Lin (M'05) received the B.S. degree from Xi'an Jiaotong University, Xi'an, China, the M.S. degree from Shandong University, Jinan, China, and the Ph.D. degree from Tsinghua University, Beijing, China, in 1997, 2000, 2004, respectively, all in electrical engineering.

He is currently a Professor in the School of Electrical Engineering, Beijing Jiaotong University, Beijing, China. His research interests include traction converter and motor drives, energy management for railway systems, digital control of power- electronic-based devices.